J|A|C|S
ARTICLES

Published on Web 11/22/2010

Dependence of Electrochemical and Electrogenerated Chemiluminescence Properties on the Structure of BODIPY Dyes. Unusually Large Separation between Sequential Electron Transfers

Alexander B. Nepomnyashchii, Sangik Cho, Peter J. Rossky, and Allen J. Bard*

Center for Electrochemistry and Chemistry and Biochemistry Department, The University of Texas at Austin, Austin, Texas 78712, United States

Received September 8, 2010; E-mail: ajbard@mail.utexas.edu

Abstract: Electrochemistry and electrogenerated chemiluminescence (ECL) of selected substituted BODIPY (4,4-difluoro-4-bora-3a,4a-diaza-*s*-indacene) dyes have been studied. The location and nature of substituents on positions 1−8 are important in predicting the behavior, and especially the stability, of the radical ions formed on electron transfer. Dyes with unsubstituted positions 2, 6, and 8 show a kinetic contribution to both oxidation and reduction. Dyes with only unsubstituted positions 2 and 6 and a substituted 8 position show chemically reversible reduction but irreversible oxidation. Unsubstituted positions 2 and 6 tend to show dimer formation on oxidation. Completely substituted dyes show nernstian oxidation and reduction. Oxidation and reduction studies of simple BODIPY dyes show an unusually large separation between the first and second reduction peaks and also the first and second oxidation peaks, of about 1.1 V, which is very different from that observed for polycyclic hydrocarbons and other heteroaromatic compounds, where the spacing is usually about 0.5 V. Electronic structure calculations confirmed this behavior, and this effect is attributed to a greater electronic energy required to withdraw or add a second electron and a lower relative solvation energy for the dianion or dication compared with those of the polycyclic hydrocarbons. ECL was generated for all compounds either by annihilation or by using a co-reactant.

1. Introduction

We report the electrochemical behavior and electrogenerated chemiluminescence (ECL) of different commercially available BODIPY (4,4-difluoro-4-bora-3a,4a-diaza-*s*-indacene) compounds (dyes). BODIPY dyes have been widely investigated[1−17] and have application as fluorescent labels for proteins and other biological materials.[4,12] They are also widely used as laser dyes.[1−3] They are interesting because their spectroscopic properties are strongly dependent on the location and nature of substituents; for example, different fluorescence emission wavelengths can be attained by making small changes in the structure[4,7,9,22] A wide range of BODIPY dyes have been synthesized with photoluminescence (PL) emission over a range of 480−700 nm.[4]

Scheme 1. Structural Representation of the BODIPY Core

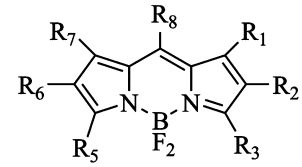

In this work we investigated the electrochemical and ECL behavior of BODIPY dyes with different substituents present. The numbering of the substituents is shown in Schemes 1 and 2 along with the structures of the compounds investigated. Some of the photophysical and electrochemical properties of these

(1) Sathyamoorthi, G.; Boyer, J. H.; Allik, T. H.; Chandra, S. *Heteroat. Chem.* **1994**, *5*, 403–407.
(2) Allik, T. H.; Hermes, R. E.; Sathyamoorthi, G.; Boyer, J. H. *Proc. SPIE-Int. Soc. Opt. Eng.* **1994**, *2115*, 240–248.
(3) Boyer, J. H.; Haag, A. M.; Sathyamoorthi, G.; Soong, M.-L.; Thangaraj, K.; Pavlopoulos, T. G. *Heteroat. Chem.* **1993**, *4*, 39–49.
(4) Loudet, A.; Burgess, K. *Chem. Rev.* **2007**, *107*, 4891–4932.
(5) Liu, J. Y.; Yeung, H. S.; Xu, W.; Li, X.; Ng, D. K. P. *Org. Lett.* **2008**, *10*, 5421–5424.
(6) Zrig, S.; Remy, P.; Andrioletti, B.; Rose, E.; Asselberghs, I.; Clays, K. *J. Org. Chem.* **2008**, *73*, 1563–1566.
(7) Ulrich, G.; Ziessel, R.; Harriman, A. *Angew. Chem., Int. Ed.* **2008**, *47*, 1184–1201.
(8) Li, Z.; Bittman, R. J. *J. Org. Chem.* **2007**, *72*, 8376–8382.
(9) Wakamiya, A.; Sugita, N.; Yamaguchi, S. *Chem. Lett.* **2008**, *37*, 1094–1095.
(10) Karolin, J.; Johansson, L. B.-A.; Strandberg, L.; Ny, T. J. *J. Am. Chem. Soc.* **1994**, *116*, 7801–7806.
(11) Wagner, R. W.; Lindsey, J. S. *Pure Appl. Chem.* **1996**, *68*, 1373–1380.
(12) Yee, M.-C.; Fas, S. C.; Stohlmeyer, M. M.; Wandless, T. J.; Climprich, K. A. *J. Biol. Chem.* **2005**, *280*, 29053–29059.
(13) Tan, K.; Jaquinod, L.; Paolesse, R.; Nardis, S.; Di Natale, C.; Di Carlo, A.; Prodi, L.; Montalti, M.; Zaccheroni, N.; Smith, K. M. *Tetrahedron* **2004**, *60*, 1099–1106.
(14) Liras, M.; Prieto, J. B.; Pintado-Sierra, M.; Arbeloa, F. L.; Garcia-Moreno, I.; Costela, A.; Infantes, L.; Sastre, R.; Amat-Guerri, F. *Org. Lett.* **2007**, *9*, 4183–4186.
(15) Pavlopoulos, T. G.; Shah, M.; Boyer, J. H. *Appl. Opt.* **1988**, *27*, 4998–4999.
(16) Pavlopoulos, T. G.; Shah, M.; Boyer, J. H. *Opt. Commun.* **1989**, *70*, 425–427.
(17) Forstner, M. B.; Yee, C. K.; Parikh, A. N.; Groves, J. T. *J. Am. Chem. Soc.* **2006**, *128*, 15221–15227.

10.1021/ja108108d

Scheme 2. Chemical Structures of the Dyes Used[a]

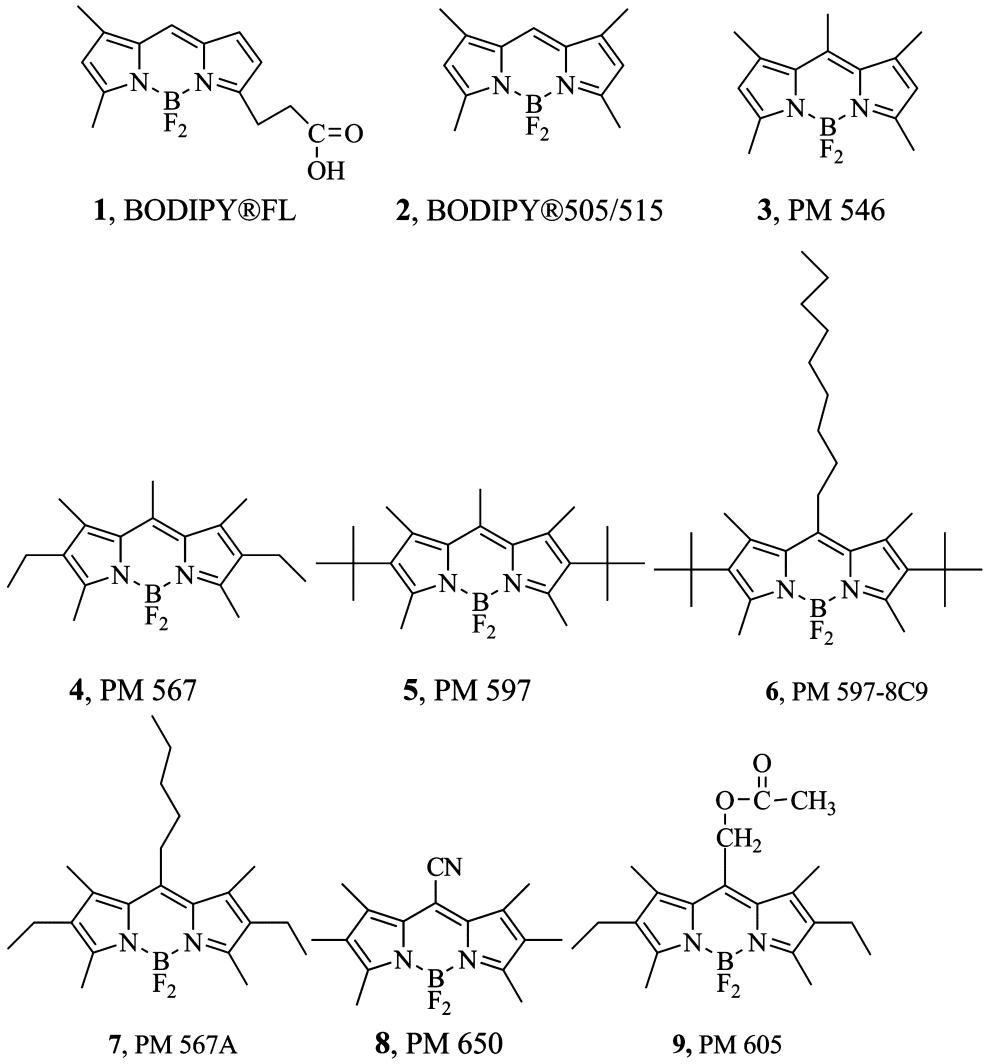

[a] **1**, 4,4-difluoro-5,7-dimethyl-4-bora-3a,4a-diaza-*s*-indacene-3-propionic acid; **2**, 4,4-difluoro-1,3,5,7-tetramethyl-4-bora-3a,4a-diaza-*s*-indacene; **3**, 4,4-difluoro-1,3,5,7,8-pentamethyl-4-bora-3a,4a-diaza-*s*-indacene; **4**, 4,4-difluoro-1,3,5,7,8-pentamethyl-2,6-diethyl-4-bora-3a,4a-diaza-*s*-indacene; **5**, 4,4-difluoro-1,3,5,7,8-pentamethyl-2,6-*tert*-butyl-4-bora-3a,4a-diaza-*s*-indacene; **6**, 4,4-difluoro-1,3,5,7-tetramethyl-2,6-*tert*-butyl-8-nonyl-4-bora-3a,4a-diaza-*s*-indacene; **7**, 4,4-difluoro-1,3,5,7-tetramethyl-2,6-diethyl-8-pentyl-4-bora-3a,4a-diaza-*s*-indacene; **8**, 4,4-difluoro-1,2,3,5,6,7-hexamethyl-8-cyano-4-bora-3a,4a-diaza-*s*-indacene; and **9**, 4,4-difluoro-1,3,5,7-tetramethyl-2,6-diethyl-8-acetoxymethyl-4-bora-3a,4a-diaza-*s*-indacene.

compounds have already been investigated,[18−21] and this work gives a broader and systematic overview of the electrochemical properties of the BODIPY molecules under the same experimental conditions. We seek to design compounds as ECL labels for biological materials and to develop guidelines for the electrochemical synthesis of BODIPY-based polymers. Chemical synthesis of such compounds for applications has already been broadly developed.[1−17,22−26]

Studies of reduction to the dianion and oxidation to the dication and the relative potentials for addition or removal of a second electron can also give insight into the behavior of these compounds.[27−37] Most of the previous electrochemical studies

(18) Lai, R. Y.; Bard, A. J. *J. Phys. Chem. B* **2003**, *107*, 5036–5042.
(19) Sartin, M. M.; Camerel, F.; Ziessel, R.; Bard, A. J. *J. Phys. Chem. C* **2008**, *112*, 10833–10841.
(20) Nepomnyashchii, A. B; Bröring, M.; Ahrens, J.; Krüger, R.; Bard, A. J. *J. Phys. Chem. C* **2010**, *114*, 14453–14460.
(21) Benniston, A. C.; Copley, G.; Lemmetyinen, H.; Tkachenko, N. V. *Eur. J. Org. Chem.* **2010**, 2867–2877.
(22) Arbeloa, T. L.; Arbeloa, F. L.; Arbeloa, I. L.; Garcia-Moreno, I.; Costela, A.; Sastre, R.; Amat-Guerri, F. *Chem. Phys. Lett.* **1999**, *299*, 315–321.
(23) Kim, B.; Ma, B.; Donuru, V. R.; Liu, H.; Freschet, J. M. J. *Chem. Commun.* **2010**, *46*, 4148–4150.
(24) Kennedy, D. P.; Kormos, C. M.; Burdette, S. *J. Am. Chem. Soc.* **2009**, *131*, 8578–8586.
(25) Forgie, J.; Skabara, P. J.; Stibor, I.; Viela, F.; Vobecka, Z. *Chem. Mater.* **2009**, *21*, 1784–1786.
(26) Bouit, P. A.; Kamada, K.; Feneyrou, P.; Berginc, G.; Toupet, L.; Maury, O.; Andraud, C. *Adv. Mater.* **2009**, *21*, 1151–1154.
(27) Aten, A. C.; Burthker, C.; Hoytink, G. J. *Trans. Faraday Soc.* **1959**, *55*, 324–330.
(28) Bard, A. J.; Santhanam, K. S. V. *J. Am. Chem. Soc.* **1966**, *88*, 2669–2675.
(29) Bard, A. J. *Pure Appl. Chem.* **1971**, *25*, 379–394.
(30) Hoytink, G. J. In *Advances in Electrochemistry and Electrochemical Engineering*; Delahay, P., Ed.; Wiley Interscience: New York, 1970; Vol. 7 and references therein.
(31) Maloy, J. T.; Bard, A. J. *J. Am. Chem. Soc.* **1971**, *93*, 5968–5981.
(32) Meerholz, K.; Heinze, J. *J. Am. Chem. Soc.* **1989**, *111*, 2325–2326.
(33) Dietz, R.; Larcombe, B. E. *J. Chem. Soc. B* **1970**, 1369–1373.
(34) Tokel, N. E.; Keszthelyi, C. P.; Bard, A. J. *J. Am. Chem. Soc.* **1972**, *94*, 4872–4877.
(35) Paquette, L. A.; Ley, S. V.; Meisinger, R. H.; Russell, R. K.; Oku, M. *J. Am. Chem. Soc.* **1974**, *96*, 5806–5815.

of BODIPY dyes were concerned only with the first oxidation and reduction waves in the potential range of about −1.3 to 1.3 V vs SCE.[38−40] Numerous studies of aromatic hydrocarbons have shown that the separation between waves is typically about 0.5 V. This results from the additional energy needed to remove an electron from a more positively charged species in $R^+ \rightarrow R^{2+}$ (or to add an electron in $R^- \rightarrow R^{2-}$) and the differences in solvation energy between the species. However, we show here that for the BODIPY compounds this difference is greater than 1.0 V. Density functional theory (DFT) and semiempirical electronic structure methods combined with a continuum solvent description of solvation are used to interpret this result.

2. Experimental Section

2.1. Chemicals. The dyes of interest **1** and **2** were obtained from Invitrogen (Eugene, OR). All other dyes were obtained from Exciton, Inc. (St. Louis, MO). IUPAC names of these compounds are given in the caption of Scheme 2. Tris(2,2′-bipyridyl)ruthenium(II) dichloride hexahydrate ($Ru(bpy)_3Cl_2 \cdot 6H_2O$), anhydrous acetonitrile (MeCN, 99.93%), dichloromethane (DCM, 99.3%), and tri-*n*-propylamine (99%) were from Aldrich Chemical Co. (Milwaukee, WI) and used as received. Electrochemical-grade supporting electrolyte tetra-*n*-butylammonium hexafluorophosphate ($TBAPF_6$) and benzoyl peroxide were obtained from Fluka (Milwaukee, WI) and used without further purification. Tetrahydrofuran (THF) was purified prior to the experiment by using a Vacuum Atmospheres solvent purification system (Vacuum Atmospheres Corp., Hawthorne, CA).

2.2. Apparatus and Methods. UV−vis absorbance and fluorescence measurements were carried out in DCM solutions under air-saturated conditions, and the quantum yield was determined and compared with the literature results for dyes using fluorescein as a standard. UV−vis spectra were recorded using a 1 cm quartz cuvette on a DU 640 spectrophotometer (Beckman, Fullerton, CA). Fluorescence spectra were recorded by using a double-beam QuantaMaster spectrophotofluorimeter (Photon Technology International, Birmingham, NJ). A 70 W Xe lamp was used as the light source for the excitation, and the slits were set at 0.5 mm. All electrochemical experiments were done under anhydrous conditions. DCM was used for all first-electron studies, and THF and MeCN were used for second-electron-transfer investigations. All solutions were prepared in a helium atmosphere drybox (Vacuum Atmospheres Corp.). After preparation, the solution was sealed in a glass cell with a Teflon cap. A 0.0314 cm^2 Pt disk, oriented downward, working electrode was used for the cyclic voltammetry (CV) experiments, and an L-shaped Pt electrode with the same area was used for the ECL spectra experiments. The working electrode was polished after each experiment with 0.3 μm alumina (Buehler, Ltd., Lake Bluff, IL) for several minutes, sonicated in ethanol and in water for 5 min, and dried in an oven at 120 °C. A Ag wire quasi-reference electrode and a Pt wire as a counter electrode were used. Potentials in CV were calibrated with ferrocene as a standard, taking $E^{\circ\prime} = 0.342$ V vs SCE.[41] The diffusion coefficient was determined from the scan rate dependence using the Randles−Ševčik equation and from chronoamperometric pulsing for 1 s using the Cottrell equation. CV and chronoamperometry measurements were carried out with a CHI 660 electrochemical workstation (CH Instruments, Austin, TX). ECL spectra were generated by using both CHI 660 and Eco Chemie Autolab PGSTAT30 potentiostats (Utrecht, The Netherlands), and the ECL transients and simultaneous CV and ECL measurements were obtained by using the Autolab instrument, which has several channels. ECL spectra for the annihilation were recorded by pulsing the potential with a pulse width of 0.1 s from about 80 mV past the peaks' potentials for 1 min. The slit width was set to 0.5 cm. All spectra were collected with a Princeton Instruments Spec-10 CCD camera (Trenton, NJ) with an Acton SpectraPr-150 monochromator (Acton, MA). Prior to the experiments, the wavelength scale of the instrument was calibrated by using a Hg/Ar pen-ray lamp from Oriel (Stratford, CT). ECL intensity signals were detected by a photomultiplier tube (PMT, Hamamatsu R4220, Japan), which was connected with a KEPCO Inc. (Vicksburg, MI) high-voltage power supply operated at −750 V. An electrometer (model 6517, Keithley Instruments Inc., Cleveland, OH) was used to collect the ECL signal from the PMT. The ECL signal was recorded simultaneously with the CV data using the Autolab, which was connected to the electrometer. ECL intensities were compared to those for 1 mM $Ru(bpy)_3^{2+}$. Digital simulations were carried out by using Digisim software (Bioanalytical Systems, West Lafayette, IN).[42−45]

Scheme 3. Thermodynamic Cycle Connecting the Oxidized (O) and the Reduced (R) States in a Solvent

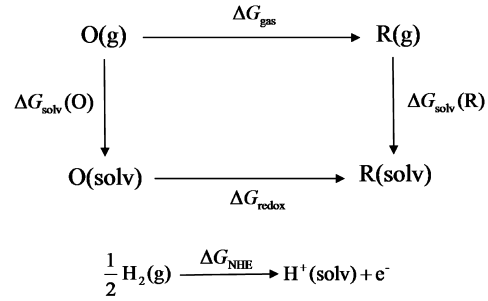

2.3. Calculations. The reduction potentials of various charge states of dyes **4** and **7** and 9,10-diphenylanthracene were calculated and compared to the experimental values. The reduction steps subject to the calculations are ox2 (+2 charge) → ox1 (+1 charge), ox1 → neu (neutral), neu → re1 (−1 charge), and re1 → re2 (−2 charge). The free energy difference between reduced and oxidized states of a chemical in acetonitrile was divided into separate steps via the equivalent thermodynamic cycle in Scheme 3, and the free energy related to each step was calculated using appropriate approximations. This kind of approach has been used for various oxygen- or sulfur-centered organic radicals of small size.[46] In addition, larger systems were tested to show that the approach can be useful for these.[47]

The standard reduction potential E° of a redox reaction $O + ne^- \rightarrow R$ is related to the free energy difference (R, reduced; O, oxidized),

$$\Delta G_{\text{redox}} = G(\text{R}) - G(\text{O}) \quad (1)$$

$$\Delta G_{\text{redox}} - n\Delta G_{\text{NHE}} = -nFE^\circ \quad (2)$$

where F is the Faraday constant, $\Delta G_{\text{NHE}} = -4.43$ eV is the absolute potential of the normal hydrogen electrode (NHE), and E° is the reduction potential measured relative to NHE. The reduction

(36) Thielen, D. R.; Anderson, L. B. *J. Am. Chem. Soc.* **1972**, *94*, 2521–2523.
(37) Müllen, K. *Chem. Rev.* **1984**, *84*, 603–646.
(38) Kollmannsberger, M.; Gareis, T.; Heinl, S.; Breu, J.; Daub, J. *Angew. Chem., Int. Ed.* **1997**, *36*, 1333–1335.
(39) Trieflinger, C.; Röhr, H.; Rurack, K.; Daub, J. *Angew. Chem., Int. Ed.* **2005**, *44*, 6943–6947.
(40) Röhr, H.; Trieflinger, C.; Rurack, K.; Daub, J. *Chem. Eur. J.* **2006**, *12*, 689–700.
(41) Sahami, S.; Weaver, M. *J. Electroanal. Chem.* **1981**, *122*, 155–170.
(42) Rudolph, M. *J. Electroanal. Chem.* **1991**, *314*, 13–22.
(43) Rudolph, M. *J. Electroanal. Chem.* **1992**, *338*, 85–98.
(44) Mocak, J.; Feldberg, S. W. *J. Electroanal. Chem.* **1997**, *378*, 31–37.
(45) Feldberg, S. W.; Goldstein, C. I.; Rudolph, M. *J. Electroanal. Chem.* **1996**, *413*, 25–36.
(46) Schmidt am Busch, M.; Knapp, E. W. *J. Am. Chem. Soc.* **2005**, *127*, 15730–15737.
(47) Cho, S. Ph.D. Thesis, The University of Texas at Austin: Austin, TX, 2009; Chapter 4.

potentials referenced to the standard calomel electrode (SCE) are obtained by adding 0.241 eV to the corresponding value for NHE.[48]

ΔG_{gas} is the difference between the molecular free energies of redox pair O and R in a vacuum. $\Delta G_{solv}(A)$, the solvation energy, is the free energy difference in the process of moving a generic species, A, from a vacuum to a solvent. Therefore, the above equations can be expressed as

$$nFE^{\circ} = -\Delta G_{gas} - \Delta\Delta G_{solv} + n\Delta G_{NHE} \quad (3)$$

$$\Delta G_{gas} = G_{gas}(R) - G_{gas}(O) \quad (4)$$

$$\Delta\Delta G_{solv} = \Delta G_{solv}(R) - \Delta G_{solv}(O) \quad (5)$$

where ΔG_{gas} is the gas free energy and $\Delta\Delta G_{solv}$ is the solvation free energy difference between the reduced (R) and oxidized (O) states.

For the evaluation of ΔG_{gas}, the molecular free energy $G_{gas}(A)$ can be expressed as

$$G_{gas}(A) = \varepsilon_{elec} + G_{TVR}^{T=298\,K} \quad (6)$$

where ε_{elec} is the electronic energy and $G_{TVR}^{T=298\,K}$ is the summation of zero-point vibrational energy and the temperature-dependent contributions from the translational, vibrational, and rotational degrees of freedom.

2.4. Methods. 2.4.1. Geometry Optimization and Molecular Free Energy in the Gas Phase. For all molecules in this study, the equilibrium geometry in each electronic state is obtained with semiempirical AM1 ground-state energy optimization using the GAMESS program.[49,50] For even-number electron systems, the restricted Hartree−Fock (RHF) AM1 Hamiltonian is used for the singlet state, and for odd-number electron systems, the unrestricted Hartree−Fock (UHF) AM1 Hamiltonian is used for the doublet state. From the equilibrium geometries obtained, the normal modes are analyzed, and with the ideal gas, rigid rotor, and harmonic normal mode approximations, the molecular free energy ($G_{TVR}^{T=298\,K}$) is obtained. The DFT electronic energy with B3LYP functional and 6-31G(d,p) basis set for the same geometry is obtained for ε_{elec}.

2.4.2. Atomic Partial Charge Distribution for the Solvation Term. The solvation energy (ΔG_{solv}) is obtained from the electrostatic field of a solute species in a dielectric continuum solvent model. The charge distribution of the solute molecule at the AM1 geometries obtained above is calculated with DFT (B3LYP, 6-31G(d,p)) wave functions and the restrained electrostatic potential (RESP) procedure.[51]

2.4.3. Solvation Energy. Poisson's equation is solved with the DelPhi program.[52,53] The dielectric constant inside the solute volume is set to 1, and the dielectric constant $\epsilon_{MeCN} = 37.5$ is used for MeCN solvation. The boundary of the solute and solvent is defined with solvent probe radii of 2.0 Å for MeCN. For solving the Poisson equation, a focusing procedure is applied. For the initial electrostatic potential, the box size prescribing the computed domain is set so that the molecule occupies 10% of the box size with 1.0 Å grid size. In the refining step, the box size changes so that the molecule occupies 40% of the box size with 0.25 Å grid size. The solute atomic radii used with MeCN are 1.725, 2.1, 1.7, 1.7, 1.2, and 2.3 Å for C, Cl, O, N, H, and S, respectively,[46] and 1.7 and 1.6 for B and F, respectively.

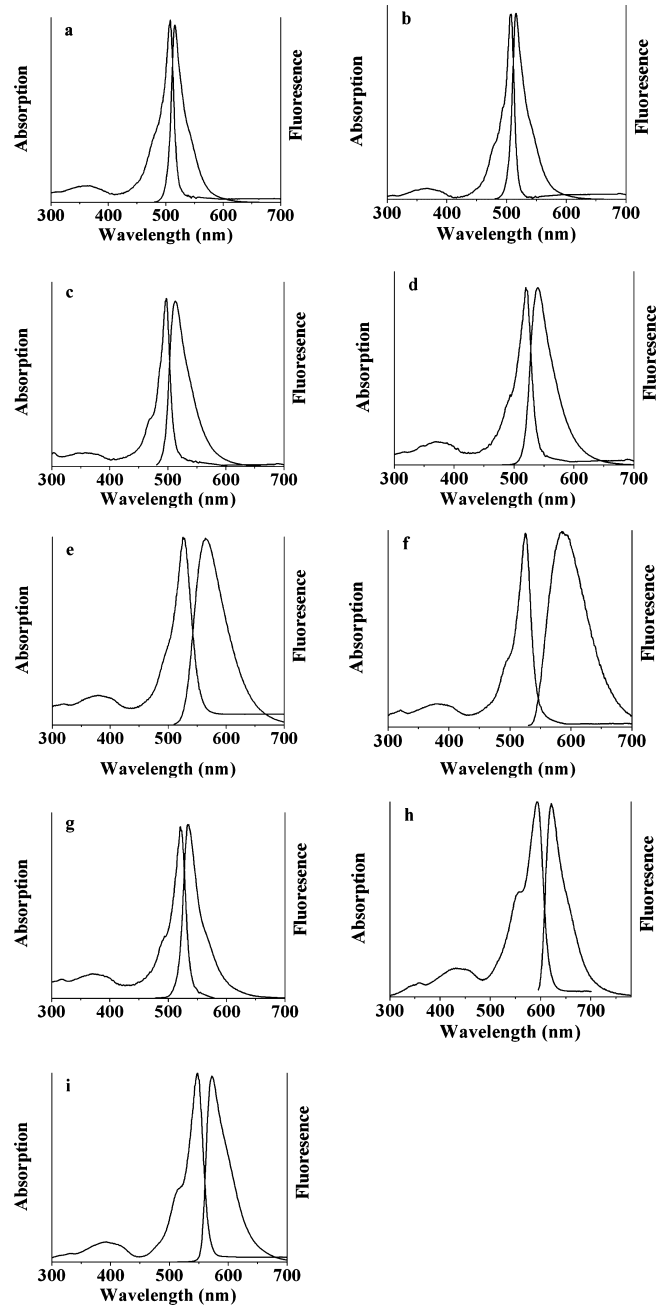

Figure 1. Absorption and fluorescence spectra of 2 μM BODIPY dyes in DCM: (a) **1**, (b) **2**, (c) **3**, (d) **4**, (e) **5**, (f) **6**, (g) **7**, (h) **8**, and (i) **9**.

3. Results

3.1. Photophysical Studies. Photophysical studies of the selected BODIPY dyes were carried out for all dyes and are shown in Figure 1 and Table 1. Fluorescence and absorbance transitions are presented in Table 1 in terms of λ and E_s (fluorescence energy). All of the compounds showed high fluorescence quantum yields, Φ_{fluor}; these were highest for the green and yellow fluorescent dyes and lower for the red fluorescent alkyl-substituted dye molecules and in the presence of the cyano group. Dyes without substitution in positions 2 and 6 (**1**−**3**) show green PL (Figure 1a−c). Addition of alkyl

(48) Reiss, H.; Heller, A. J. *J. Phys. Chem.* **1985**, *89*, 4207–4213.
(49) Dewar, M. J. S.; Zoebisch, E. G.; Healy, E. F.; Stewart, J. J. P. *J. Am. Chem. Soc.* **1985**, *107*, 3902–3909.
(50) Schmidt, M. W.; Baldridge, K. K.; Boatz, J. A.; Elbert, S. T.; Gordon, M. S.; Jensen, J. H.; Koseki, S.; Matsunaga, N.; Nguyen, K. A.; Su, S. J.; Windus, T. L.; Dupius, M.; Montgomery, J. A. *J. Comput. Chem.* **1993**, *14*, 1347–1363.
(51) Besler, B. H.; Merz, K. M.; Kollman, P. A. *J. Comput. Chem.* **1990**, *11*, 431–439.
(52) Bayly, C. I.; Cieplak, P.; Cornell, W. D.; Kollman, P. A. *J. Phys. Chem.* **1993**, *97*, 10269–10280.
(53) Nicholls, A.; Honig, B. *J. Comput. Chem.* **1991**, *12*, 435–445.

Table 1. Absorption and Fluorescent Properties of the Selected Dyes

	λ_{max} (nm)				
dye	abs	fluor	$\varepsilon \times 10^4$ (M^{-1} cm^{-1})	Φ_{fluor}	E_s (eV)
1	352, 506	515	0.74, 8.2	0.99	2.41
2	352, 505	515	0.71, 7.9	0.98	2.41
3	360, 496	512	0.70, 7.9	0.99	2.42
4	371, 521	538	0.68, 7.5	0.99	2.31
5	379, 527	566	0.60, 6.8	0.75	2.19
6	386, 524	588	0.60, 5.2	0.50	2.11
7	368, 520	532	0.79, 8.4	0.99	2.33
8	432, 596	623	0.79, 4.6	0.50	1.99
9	385, 549	572	0.68, 6.8	0.92	2.17

substitution to these positions causes a bathochromic shift of the absorbance and fluorescence spectra. Methylation of positions 2 and 6 caused a red shift of the fluorescence from green to yellow (**4** and **7**) due to the stabilization of the excited state through a positive inductive effect (Figure 1d,g). Addition of the bulkier *tert*-butyl substituents to positions 2 and 6 caused an even larger spectral red shift (**5** and **6**) and also a larger Stokes shift compared with methylated dyes as a result of the geometric restrictions (Figure 1e,f). Dyes **5** and **6** also showed broader emission, which can be taken as evidence of a larger degree of steric interactions in the system. Contrary to this, alkylation of the meso position does not have a substantial effect on the spectra. There is a small blue-shift with addition of a donating group, although this effect depends on the molecular structure.[4] The spectroscopic properties of the *meso*-cyanide dye **8** are special due to the high red-shift as compared with nonsubstituted compounds that occurs by simply changing substitution in one position (Figure 1h). The cyano group is an electron acceptor and can provide stabilization of the LUMO state, causing a decrease in the energy band gap. This shift was only seen for addition of the cyano group to the meso position, since its presence in positions 2 and 6 results in an emission wavelength that is very close to that of the corresponding alkyl derivatives.[4] The effect of the cyano group on the fluorescence is opposite to the effect of donor methyl groups. Dye **9** has an acetoxymethyl group in its structure in the meso position (Figure 1i). This dye showed relatively high fluorescent activity, with a maximum at 575 nm and an intermediate Stokes shift of 32 nm.

3.2. Electrochemical Studies of the BODIPY Dyes. 3.2.1. Electrochemical Properties. Cyclic voltammograms of the dyes are shown, for initial scans toward negative and positive potentials, in Figures 2−4, 5a,b, and 7 and Supporting Information Figure S1. The potentials of the first reduction and oxidation waves, diffusion coefficients (D), and ECL parameters (discussed later) are summarized in Table 2.

Electrochemical studies of the totally substituted dyes **4**−**7** show reversible reduction and oxidation waves in both positive and negative directions with peaks near −1.4 and 1.3 V that depend slightly on the substituent present (Figure 2). The cyclic voltammograms are for initial scans in the negative direction. Experiments with initial scans in the positive direction do not show the appearance of any additional peaks; the results are presented in Figure S2 in the Supporting Information. There is a slightly smaller separation between the oxidation and reduction peaks for dyes **5** and **6** containing *tert*-butyl groups. Thus, both radical anion and cation are quite stable because of the substituents, which block dimerization and attack by nucleophilic and electrophilic species.

Cyclic voltammograms of dye **8** show reversible reduction with $E_{1/2} = -0.82$ V and reversible oxidation with $E_{1/2} = 1.14$ V (Figure 3a). The addition of the acceptor cyano group in the 8 position makes this species much easier to reduce by about 0.4−0.5 V. This corresponds fairly well with the photophysical properties and longer emission wavelength for **8**. Dye **9**, with an acetoxymethyl substituent in the 8 position, shows high stability on oxidation but instability on reduction because of electron transfer to the substituent (Figure 3b). This produces an additional 1e reduction wave with a peak at −1.2 V, which is earlier than the next BODIPY wave with a peak at −1.42 V. There is also an additional small oxidation peak at 0.1 V when the potential is first scanned in the negative direction that is not present on an initial positive scan. This is therefore from products of the reduction. The additional waves could correspond to ester decomposition products that are sometimes seen for aromatic esters.[54] However, simple alkyl esters are usually not oxidized easily.

Both oxidation and reduction for dye **1**, which is unsubstituted in positions 1, 2, 6, and 8, are electrochemically irreversible (Figure 4a). No electrochemical waves were observed that were attributable to the reduction of propionic acid in the studied range. Dye **2**, with positions 2, 6, and 8 missing, shows behavior similar to that of **1**, with slightly higher reversibility on the oxidation because of the presence of the substitution in position 1 (Figure 4b). There is also a noticeably higher degree of irreversibility on reduction with higher concentrations of the dye, with formation of a surface wave around 0 V (Figure 5a,b). Reduction behavior can be simulated by assuming an electrochemical mechanism with a kinetic constant of 2 s^{-1} (Figure 5c−f). There is no evidence of coupling processes on reduction, such as concentration-dependent CV behavior. However, on oxidation, the appearance of a second wave while scanning to further positive potentials and concentration dependence can be seen as evidence for a coupling reaction (Figure 6). A dimerization mechanism with a coupling constant of 400 M^{-1} s^{-1} is proposed as the reaction mechanism and fitted to digital simulations:

$$\text{R-H}_2 \rightarrow \text{R-H}_2^{\bullet+} + \text{e} \qquad E^1_{1/2} = 1.11\ \text{V} \tag{7}$$

$$\text{R-H}_2^{\bullet+} + \text{R-H}_2^{\bullet+} \rightarrow \text{H}_2\text{R-RH}_2^{2+} \qquad k_{\text{dim}} = 400\ \text{M}^{-1}\ \text{s}^{-1} \tag{8}$$

$$\text{H}_2\text{R-RH}_2^{2+} \rightarrow \text{HR-RH} + 2\text{H}^+\ \text{(fast)} \qquad k = 10^{10}\ \text{s}^{-1} \tag{9}$$

$$\text{HR-RH} \rightarrow \text{HR-RH}^{\bullet+} + \text{e} \qquad E^{\text{d}}_{1/2} = 1.27\ \text{V} \tag{10}$$

$$\text{HR-RH}^{\bullet+} \rightarrow \text{HR-RH}^{2+} + \text{e} \qquad E^2_{1/2} = 1.03\ \text{V} \tag{11}$$

Concentration dependence can be seen as a proof that oxidative coupling is responsible for the appearance of the second electrochemical wave and not just consecutive reaction with solvent.[55−57] The electrode must be continuously polished

(54) Eberson, L.; Nyberg, K. Carboxylic Acids, Esters, and Anhydrides. In *Encyclopedia of the Electrochemistry of the Elements: Organic Section*; Bard, A. J., Lund, H., Eds.; Marcel Dekker: New York, 1978; Vol. 12, p 291.
(55) Nadjo, L.; Saveant, J. M. *J. Electroanal. Chem.* **1973**, *44*, 327–366.
(56) Debad, J. D.; Morris, J. C.; Magnus, P.; Bard, A. J. *J. Org. Chem.* **1997**, *62*, 530–537.

Table 2. Electrochemical Properties of the Selected Dyes

dye	$E_{1/2}$ (V vs SCE)[a] A/A$^-$	$E_{1/2}$ (V vs SCE)[a] A/A$^+$	λ_{max} (ECL) (nm)	Φ_{ECL}[b]	ΔH_s (eV)	D ($\times 10^{-6}$ cm^2/s)
1	−1.27 (E_{pc})	1.16 (E_{pa})	532	0.0006	2.23	7.0
2	−1.22	1.11	534	0.002	2.23	7.0
3	−1.22	1.12	540	0.006	2.24	7.0
4	−1.37	0.95	551	0.21	2.22	6.6
5	−1.34	0.98	572	0.15	2.22	6.2
6	−1.31	0.99	600	0.05	2.20	6.0
7	−1.33	1.02	566, 706	0.19	2.25	6.1
8	−0.82	1.14	630	0.01	1.98	6.9
9	−1.2 (E_{pc1}), −1.42 (E_{pc2})	0.98	614	0.002	2.24	6.1

[a] $E_{1/2}$ is shown for all compounds except **1** and **9**, where E_p values are used for reduction and oxidation of **1** and reduction of **9**. [b] Relative to $Ru(bpy)_3^{2+}$ under similar conditions.

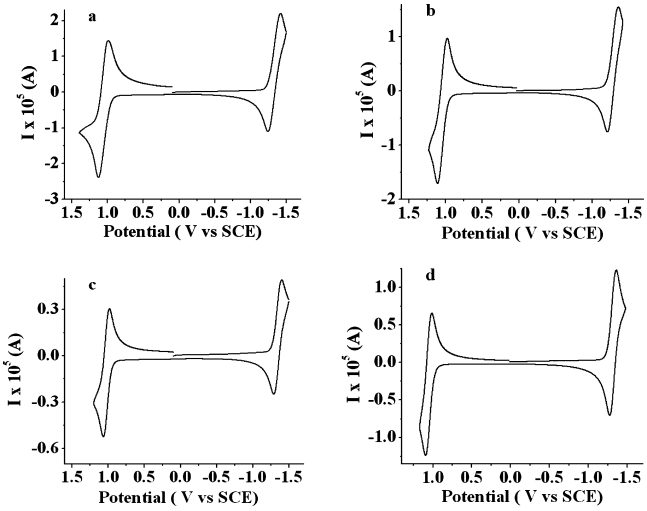

Figure 2. Cyclic voltammograms of the completely substituted BODIPY dyes **4**−**7** at a scan rate of 0.1 V/s in DCM at Pt working electrode (area = 0.0314 cm^2): (a) 3 mM **4**, (b) 2.2 mM **5**, (c) 0.6 mM **6**, and (d) 1.5 mM **7**. Supporting electrolyte, 0.1 M $TBAPF_6$. All scans start in the negative direction (scans in the positive direction are shown in the Supporting Information). As shown, the current scale encompasses ±25 μA.

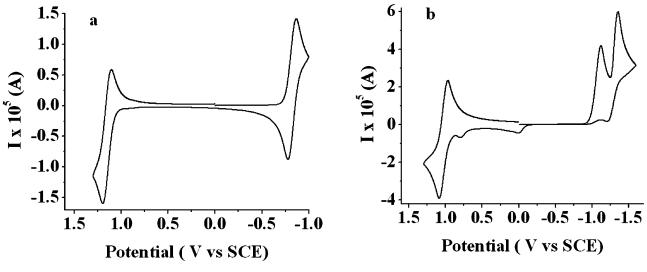

Figure 3. Cyclic voltammograms of BODIPY dyes **8** and **9** at a scan rate of 0.1 V/s in DCM at Pt working electrode (area = 0.0314 cm^2): (a) 2.5 mM **8** and (b) 7 mM **9**. Supporting electrolyte, 0.1 M $TBAPF_6$. All scans start in the negative direction (scans in the positive direction are shown in the Supporting Information). As shown, the current scale encompasses ±60 μA.

during electrochemical investigations because of the formation of a blocking film after several consecutive cycles. This may be seen as a further sign of the coupling processes. Dye **3** shows nernstian reduction but oxidation behavior similar to that of **1** and **2**, due to the presence of the methyl group in the position 8 and the absence of substitution in positions 2 and 6 (Figure 7). This confirms that missing substitution in positions 2 and 6 affects the oxidation but not the reduction.

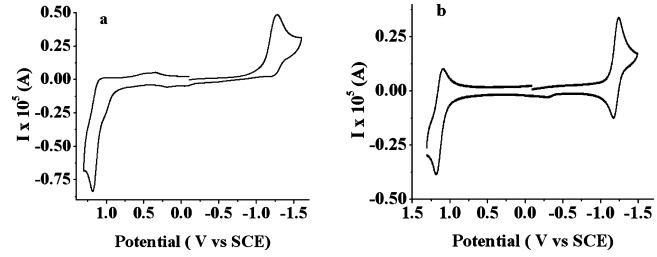

Figure 4. Cyclic voltammograms of 2,6,8-unsubstituted BODIPY dyes **1** and **2** at a scan rate of 0.1 V/s in DCM at Pt working electrode (area = 0.0314 cm^2): (a) 0.7 mM **1** and (b) 0.4 mM **2**. Supporting electrolyte, 0.1 M $TBAPF_6$. All scans start in the negative direction (scans in the positive direction are shown in the Supporting Information). As shown, the current scale encompasses ±6 μA.

3.2.2. Potential Difference between Sequential Oxidation and Reduction Waves. Oxidation and reduction scans of the dyes to more negative and more positive potentials can provide information about the energies needed to form the dianions and dications of these compounds (Figure 8a,b and Supporting Information Figure S3). Reduction of the dyes at more negative potentials generally produced a second peak attributed to the addition of a second electron. Most reduction experiments were carried out in THF because it has a wider potential range for reduction than MeCN and DCM and a higher stability of anions. All oxidations were studied in MeCN, which showed a relatively high stability of the radical cations over a wide potential window. The separation between the first and second reduction waves (ΔE_c) was 1.0−1.25 V, while that for the oxidation waves (ΔE_a) was 1.2−1.3 V for the alkyl-substituted dyes (Figure 8a,b, and Supporting Information Figure S3a−f). The second reduction and oxidation waves are irreversible, as is frequently seen with dications and dianions, except for dye **8**, where the dianion was quite stable (Supporting Information Figure S3h). One can account for this behavior due to the fact that **8** is much easier to reduce than the other dyes, and hence the wave occurs at a less negative potential. The general instability of the dianions usually involves a following homogeneous reaction that causes a shift of the waves to less extreme potentials (i.e., to more positive potentials for oxidation and more negative potentials for reduction). Reversible behavior to the dianion and clean electrochemistry at very negative potentials can be seen in liquid ammonia, but this can only increase ΔE_c.[58−61] The less negative

(57) Zhou, F.; Unwin, P. R.; Bard, A. J. *J. Phys. Chem.* **1992**, *96*, 4917–4924.

(58) Demortier, A.; Bard, A. J. *J. Am. Chem. Soc.* **1973**, *95*, 3495–3500.
(59) Smith, W. H.; Bard, A. J. *J. Am. Chem. Soc.* **1975**, *97*, 6491–6495.
(60) Smith, W. H.; Bard, A. J. *J. Am. Chem. Soc.* **1975**, *97*, 5203–5210.

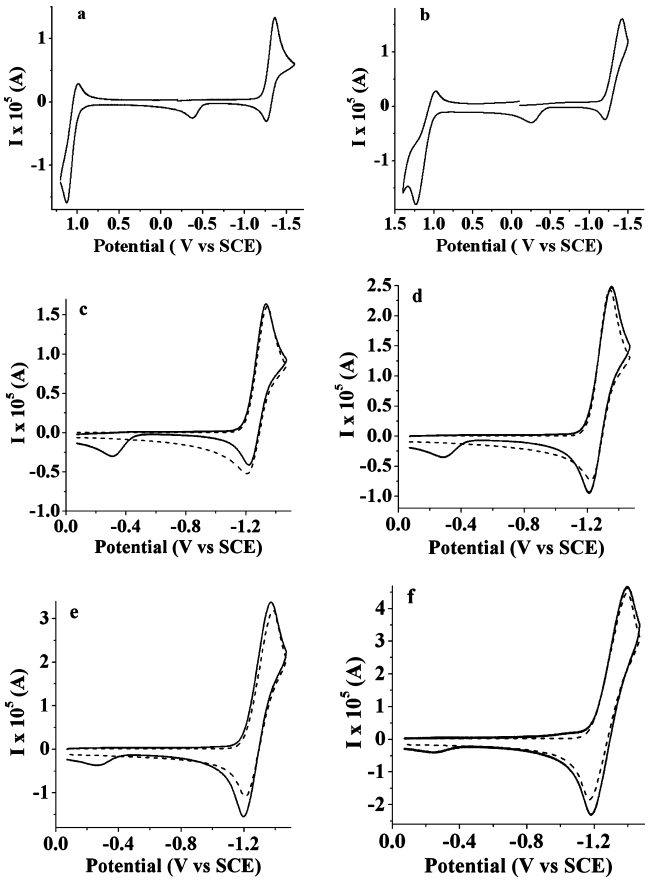

Figure 5. (a,b) Cyclic voltammograms for (a) 1.9 and (b) 2.3 mM **2**. (c−f) Experimental (solid line) and simulated parameters (dashed line) for reduction of 2.4 mM **2** at (c) 0.1, (d) 0.25, (e) 0.5, and (f) 1 V/s. Experimental data: solvent, DCM; supporting electrolyte, 0.1 M $TBAPF_6$; and electrode area, 0.0314 cm^2. Simulated data: diffusion coefficient, 7.0×10^{-6} cm^2/s; uncompensated resistance, 2000 Ω; capacitance, 3×10^{-7} F; and kinetic constant, 2 s^{-1}. As shown, the current scale encompasses ±50 μA.

reduction potential due to the presence of the cyano group made it possible to obtain both second oxidation and reduction in one solvent, acetonitrile (Supporting Information Figure S3g). The first reduction wave potentials for **8** in both THF and MeCN were about the same (referenced to Fc or SCE), suggesting about the same solvent effect on the electrochemical behavior of these dyes. Dye **9** also showed a large separation of the oxidation waves, and the reduction behavior studies were complicated because of the reduction of the acetoxymethyl prior to the reduction of the BODIPY core (Supporting Information Figure S3j). The separation between the two sequential reduction peaks for dyes **1**−**3** was also around 1.0 V, with the stability of the anions depending on the presence of a substituent in position 8 (Supporting Information Figure S3k,m,o). Dyes **1**−**3** that are unsubstituted in the 2 and 6 positions actually show three peaks on oxidation (Supporting Information Figure S3l,n,p). In addition to the formation of radical cation and dication in the first and third peaks, a second peak that is assigned to the reaction of the product of the unstable radical cation, perhaps from a dimerization reaction, is seen. Even with these compounds, the

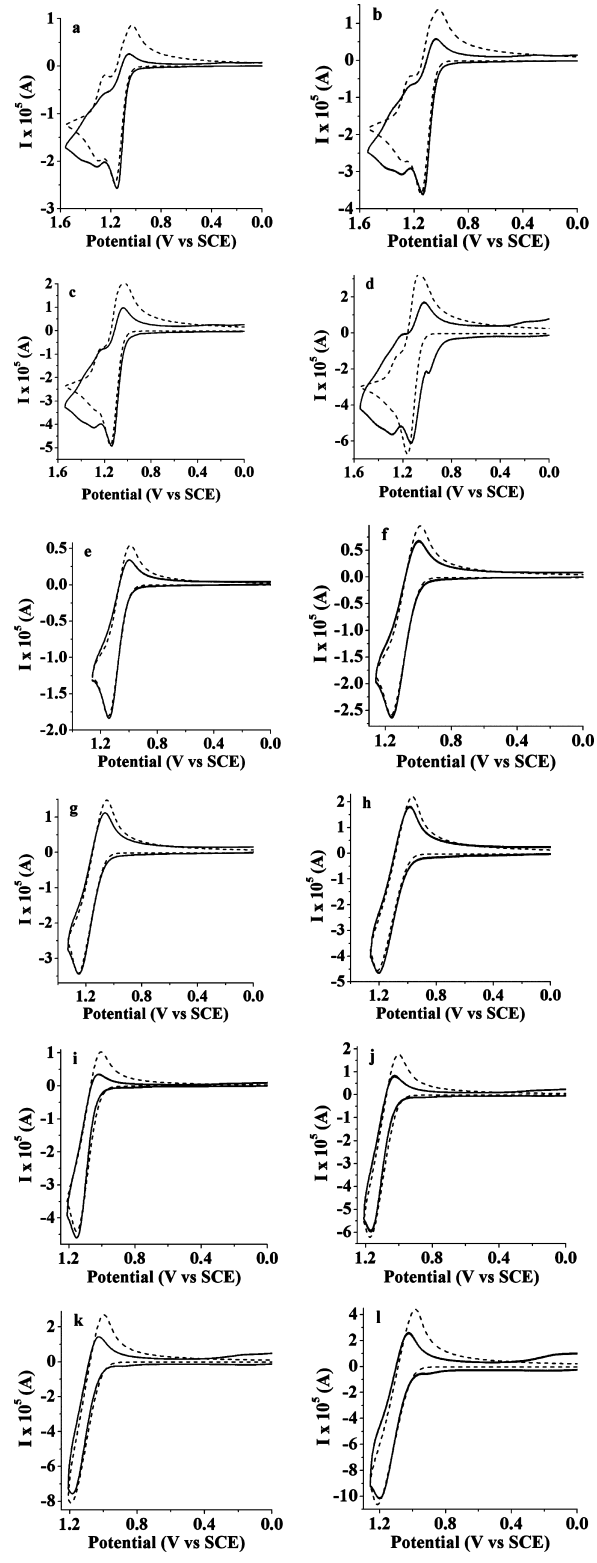

Figure 6. (a−h) Experimental (solid line) and simulated (dashed line) data for 2.4 mM at (a,e) 0.1, (b,f) 0.25, (c,g) 0.5, and (d,h) 1 V/s. (i−l) Experimental (solid line) and simulated (dashed line) data for 5.2 mM **2** at (i) 0.1, (j) 0.25, (k) 0.5, and (l) 1 V/s. Experimental data: solvent, DCM; supporting electrolyte, 0.1 M $TBAPF_6$; and electrode area, 0.0314 cm^2. Simulated data: diffusion coefficient for the monomer, 7.0×10^{-6} cm^2/s, and for the dimer, 5.2×10^{-6} cm^2/s; uncompensated resistance, 2000 (a−h) and 1000 Ω (i−l); capacitance, 3×10^{-7} F; dimerization constant, 400 M^{-1} s^{-1}; deprotonation constant, 10^{10} s^{-1}. As shown, the current scale encompasses ±110 μA.

(61) Amatore, C.; Badoz-Lambling, J.; Bonnel-Huyghes, C.; Pinson, J.; Saveant, J. M.; Thiebault, A. *J. Am. Chem. Soc.* **1982**, *104*, 1979–1986.

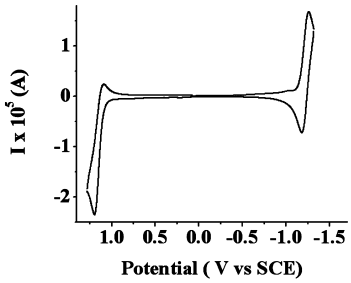

Figure 7. Cyclic voltammogram of 2.2 mM 2,6-unsubstituted BODIPY dye **3** at a scan rate of 0.1 V/s in DCM at Pt working electrode (area = 0.0314 cm^2). Supporting electrolyte, 0.1 M $TBAPF_6$. The current scan starts in the negative direction (scan in the positive direction is shown in Supporting Information). As shown, the current scale encompasses ± 20 μA.

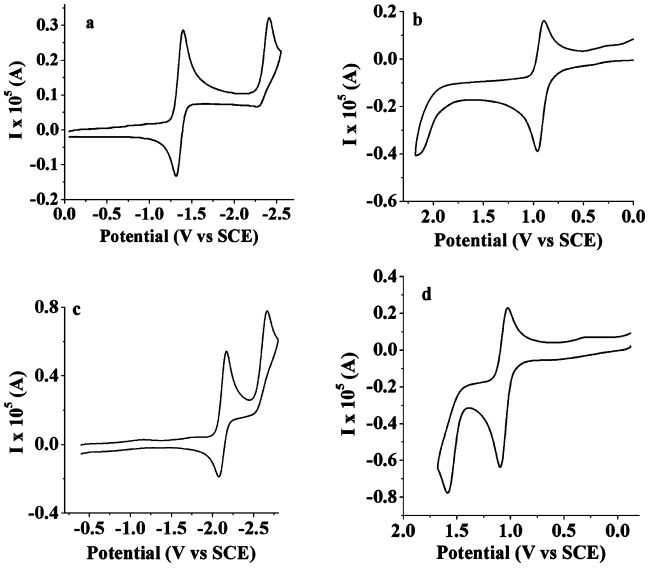

Figure 8. Cyclic voltammograms of (a,b) BODIPY dye **4** and (c,d) 9,10-diphenylanthracene at a scan rate of 0.1 V/s at Pt working electrode (area = 0.0314 cm^2). Supporting electrolyte, 0.1 M $TBAPF_6$; solvent, THF [(a) 0.5 mM **4**; (c) 1.0 mM 9,10-diphenylanthracene] or acetonitrile [(b) 0.6 mM **4**; (d) 1.0 mM 9,10-diphenylanthracene]. As shown, the current scale encompasses ± 10 μA.

Scheme 4. Chemical Structure of 9,10-Diphenylanthracene

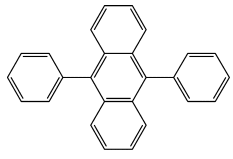

separation between the first and third oxidation waves is about 1.2 V, consistent with the other dyes with more stable radical cations.

Experiments with many other BODIPY dyes have demonstrated that an unusually large potential separation between two sequential reduction and oxidation waves is a characteristic feature of these dyes, as opposed to what is seen in general for aromatic compounds. For example, the widely investigated polycyclic hydrocarbon 9,10-diphenylanthracene (DPA) (Scheme 4) shows two oxidation and two reduction waves with the separation of 0.5 V (Figure 8c,d); this behavior is similar to the ΔE_c and ΔE_a seen for many polycyclic hydrocarbons.[28] Electronic structure calculations were carried out to investigate the cause of this unusually large splitting between waves in the

Table 3. Experimental and Calculated Reduction and Oxidation Potentials of BODIPY Core, Dyes **4** and **7**, and 9,10-Diphenylanthracene in Tetrahydrofuran (Reductions) and MeCN (Oxidations)

		electrode potential, E° (V)		calculated energy terms (eV)		
compd	half-reaction	expt[a]	calcd[b]	$\Delta\varepsilon_{elec}$[c]	$\Delta\Delta G_{solv}$[d]	ΔG_{TVR}[e]
4	ox2 → ox1	~2.3	2.31	−11.08	4.59	0.07
	ox1 → neu	0.94	0.89	−6.52	1.44	0.09
	neu → re1	−1.37	−1.67	−0.83	−1.70	0.00
	re1 → re2	~ −2.46	−3.04	3.68	−4.83	0.02
7	ox2 → ox1	~2.3	2.40	−10.99	4.40	0.07
	ox1 → neu	0.94	0.93	−6.47	1.35	0.09
	neu → re1	−1.33	−1.65	−0.87	−1.66	0.00
	re1 → re2	~ −2.42	−3.06	3.49	−4.62	0.02
DPA	ox2 → ox1	~1.7	1.71	−10.17	4.27	−0.05
	ox1 → neu	1.2	0.89	−6.38	1.30	0.08
	neu → re1	−2.1	−2.10	−0.34	−1.75	
	re1 → re2	−2.6	−2.87	3.26	−4.58	

[a] Reference to SCE obtained from 0.342 V vs SCE for ferrocene couple. [b] Reference to SCE obtained from 0.241 V vs NHE assuming aqueous system. Only $\Delta\varepsilon_{elec}$ and $\Delta\Delta G_{solv}$ are considered (ΔG_{TVR} is neglected; see eq 6). [c] The difference in electronic energies of reduced and oxidized species from DFT. Since ΔG_{TVR} is neglected, $\Delta\varepsilon_{elec} \approx \Delta G_{gas}$. [d] The difference in ΔG_{solv} of reduced and oxidized species. See text. [e] The difference in G_{TVR} of reduced and oxidized species in AM1 energy. See text.

BODIPY dyes (Table 3, Supporting Information Table S1, and Supporting Information Figures S4−S7). Calculations of the thermodynamic properties of the completely substituted compounds **4** and **7** are compared with those for DPA. These represent sterically hindered systems with relatively high electrochemical stability on both oxidation and reduction.

The calculated electrode potentials for both the reduction steps −2/−1 and −1/0 and oxidation steps +2/+1 and +1/0 agree quite well. The average differences between the first and second electrode potentials for the BODIPY compounds are as follow: experimental, 1.5 (oxidative wave) and 1.0 eV (reductive wave); calculated, 1.4 eV (for both oxidative and reductive waves). For 9,10-diphenylanthracene, the experimental values are 0.5 eV on both oxidative and reductive waves, compared to calculated values of 0.8 eV. On the basis of the calculations, one can compare the electronic (gas phase) and the solvation effects. For the BODIPY compounds, the average difference in the solvation effects (the difference in $\Delta\Delta G_{solv}$ for all splittings) is 3.1 eV, as compared to 2.9 eV for the splitting in DPA, so the solvation contribution is close to the same in both compounds, as would be expected from the similar size of the two molecules: 48 atoms for **4** and 44 for DPA. However, the difference in $\Delta\varepsilon_{elec}$ (or ΔG_{gas}), 4.5 eV for BODIPY vs 3.6 eV for DPA, is more significant. Thus, the difference in electrochemical response is mainly accounted for by differences in the electronic properties, $\Delta\varepsilon_{elec}$, that are clear in the gas phase. The other features seen in calculations are a positive charge on the boron atom, a negative charge on the nitrogens, and the relatively large electron density on the central meso atom (position 8 or atom 4 in Supporting Information Figure S5), which corresponds well with previous results (Supporting Information Figure S4).[62,63] This then rationalizes why the absence of substitution in positions 2 and 6 affects the stability

(62) Prieto, J. B.; Arbeloa, F. L.; Martinez, V. M.; Arbeloa, I. L. *Chem. Phys.* **2004**, *296*, 13–22.
(63) Prieto, J. B.; Arbeloa, F. L.; Martinez, V. M.; Lopez, T. A.; Arbeloa, I. L. *Phys. Chem. Chem. Phys.* **2004**, *6*, 4247–4253.

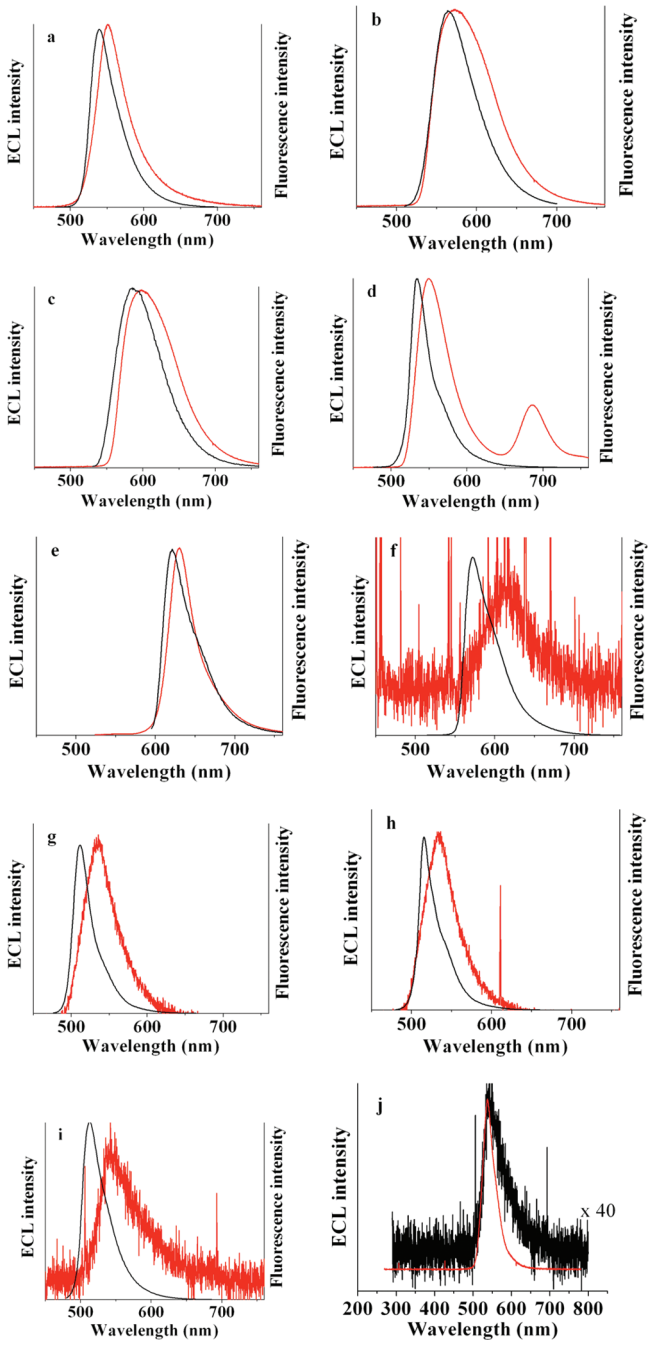

Figure 9. (a−i) ECL (red line) and fluorescence (black line) spectra for the BODIPY dyes of certain concentrations: (a) 2.2 mM **4**, (b) 2.2 mM **5**, (c) 2.2 mM **6**, (d) 2.3 mM **7**, (e) 2.2 mM **8**, (f) 2.2 mM **9**, (g) 2 mM **1**, (h) 2.3 mM **2**, and (i) 2.3 mM **3**; (a−e) annihilation-generated ECL; (f) in the presence of 0.1 M TPrA; and (g−i) in the presence of 10 mM BPO. (j) Comparison spectra of the annihilation ECL (black line) and in the presence of 10 mM BPO (red line). For all experiments, time of stepping was 1 min and frequency was 10 Hz. Annihilation ECL was done from 80 mV of the peaks; co-reactant ECL was done from 80 mV of the reduction and oxidation peaks. Solvent: (a−e,g−i) DCM and (f) acetonitrile.

of the radical cation and position 8 influences the stability of the anion radical.

3.3. Electrogenerated Chemiluminescence. Dye **4** shows very stable orange ECL emission by radical ion annihilation with a maximum at 535 nm (Figure 9a):

$$\mathrm{BODIPY} + \mathrm{e} \rightarrow \mathrm{BODIPY}^{\bullet -} \quad (12)$$

$$\mathrm{BODIPY} - \mathrm{e} \rightarrow \mathrm{BODIPY}^{\bullet +} \quad (13)$$

$$\mathrm{BODIPY}^{\bullet -} + \mathrm{BODIPY}^{\bullet +} \rightarrow {}^{1}\mathrm{BODIPY}^{*} + \mathrm{BODIPY} \quad (14)$$

$$\mathrm{BODIPY}^{\bullet -} + \mathrm{BODIPY}^{\bullet +} \rightarrow {}^{3}\mathrm{BODIPY}^{*} + \mathrm{BODIPY} \quad (15)$$

$${}^{3}\mathrm{BODIPY}^{*} + {}^{3}\mathrm{BODIPY}^{*} \rightarrow {}^{1}\mathrm{BODIPY}^{*} + \mathrm{BODIPY} \quad (16)$$

$${}^{1}\mathrm{BODIPY}^{*} \rightarrow \mathrm{BODIPY} + h\nu \quad (17)$$

The peak position of the ECL spectrum is slightly red-shifted as compared with the fluorescence spectrum due to an inner filter effect. Quantum efficiency calculations for ECL were carried out for multiple potential step annihilation experiments, and obtained values were compared with results obtained under similar conditions for $Ru(bpy)_3^{2+}$. The uncertainty of results is at least ±20%, depending on the structure of the compound, due to the possibility of fouling of the electrode from following chemical reactions. Dyes **5** and **6** show broader ECL behavior under the same conditions, comparable with the broader PL emission (Figure 9b,c). No longer wavelength emission, attributable to aggregate or reaction product formation, is seen for **6** because of the presence of the blocking *tert*-butyl groups (Figure 9c).[20] A longer wavelength band is seen with **7**, however (Figure 9d).[20] The intensity of ECL is lower for **6** compared with that for **5** but sufficient to be able to record spectra with the CCD camera. Dye **8** shows a red-shifted ECL compared with that of the alkyl-substituted dyes, as seen also in the PL results (Figure 9e). The relatively low ECL intensity for dye **8** compared with that of the methyl- or ethyl-substituted dyes can be explained by the presence of the acceptor cyano group, which increases the nonradiative decay of the excited states (Table 3). Annihilation experiments of dye **9** with reduction and oxidation at 80 mV past the peaks produced only low light intensities, insufficient to obtain spectra. Thus, TPrA was used as a co-reactant to obtain ECL spectra (Figure 9f). This low intensity of the spectrum can be caused by the unstable reduction product. The mechanism of ECL in the presence of TPrA can be represented then as[64]

$$\mathrm{BODIPY} - \mathrm{e} \rightarrow \mathrm{BODIPY}^{\bullet +} \quad (18)$$

$$\mathrm{TPrA} - \mathrm{e} \rightarrow \mathrm{TPrA}^{\bullet +} \quad (19)$$

$$\mathrm{TPrA}^{\bullet +} \rightarrow \mathrm{TPrA}^{\bullet} + \mathrm{H}^{+} \quad (20)$$

$$\mathrm{BODIPY}^{\bullet +} + \mathrm{TPrA}^{\bullet} \rightarrow {}^{1}\mathrm{BODIPY}^{*} + \mathrm{TPrA}^{+} \quad (21)$$

$${}^{1}\mathrm{BODIPY}^{*} \rightarrow \mathrm{BODIPY} + h\nu \quad (22)$$

Dyes **1** and **2** did not generate spectra, but the use of a reductive co-reactant such as benzoyl peroxide (BPO) produced ECL emission of sufficient intensity to generate spectra (Figure 9g,h). The mechanism of benzoyl peroxide can be presented as[65−67]

(64) Lai, R. Y.; Bard, A. J. *J. Phys. Chem. A* **2003**, *107*, 3335–3340.
(65) Chandross, E. A.; Sonntag, F. I. *J. Am. Chem. Soc.* **1966**, *88*, 1089–1096.
(66) Akins, D. L.; Birke, R. L. *Chem. Phys. Lett.* **1974**, *29*, 428–435.
(67) Santa Cruz, T. D.; Akins, D. L.; Birke, R. L. *J. Am. Chem. Soc.* **1976**, *98*, 1677–1682.

$$\text{BODIPY} + e \rightarrow \text{BODIPY}^{\bullet -} \quad (23)$$

$$\text{BODIPY}^{\bullet -} + \text{BPO} \rightarrow \text{BODIPY} + \text{BPO}^{\bullet -} \quad (24)$$

$$\text{BPO}^{\bullet -} \rightarrow C_6H_5CO_2^- + C_6H_5CO_2^{\bullet} \quad (25)$$

$$\text{BODIPY}^{\bullet -} + C_6H_5CO_2^{\bullet} \rightarrow {}^1\text{BODIPY}^* + C_6H_5CO_2^- \quad (26)$$

$${}^1\text{BODIPY}^* \rightarrow \text{BODIPY} + h\nu \quad (27)$$

Attempts to use the oxidative co-reactant TPrA were unsuccessful, probably because oxidation in the presence of the BODIPY dye causes oxidative coupling with film formation. Compound **1** is used as a lipid probe in the fluorescence studies, but its ECL applicability in this case is complicated by the lack of substituents leading to instability of the radical ions, which is not a factor in PL studies.[68−70] Dye **3** can generate light by an annihilation reaction, although the efficiency is much lower compared with that of co-reactant ECL as a result of the coupling process on oxidation (Figure 9i,j).[71−73] No ECL products for the dimerization were observed because of the high stability of the radical anion and also fast film formation on oxidation.

The nature of the excited state produced during ECL of the BODIPY compounds is also of interest.[74] The total energy for the annihilation can be accessed from the Gibbs free energy, $\Delta G_{ann} = \Delta H_s - T\Delta S$, where ΔH_s is the enthalpy for the annihilation and $T\Delta S$ the entropic factor, assumed to be 0.1 eV. The energies for the annihilation for dyes **1**−**9** (**1**, 2.23 eV; **2**, 2.23 eV; **3**, 2.24 eV; **4**, 2.22 eV; **5**, 2.22 eV; **6**, 2.20 eV; **7**, 2.25 eV; **8**, 1.98 eV; **9**, 2.24 eV) are all very close to the singlet energy estimated from the fluorescence results (Tables 2 and 3). The closeness suggests either a singlet or ST-annihilation route (production of both singlet and triplet excited states, followed by triplet−triplet annihilation) for the ECL. The possibility of ECL via the triplet state was shown in experiments with 10-methylphenothiazine (10-MP).[18]

4. Conclusions

The electrochemistry and ECL of a number of BODIPY dyes were studied and compared with the photophysical properties. The importance of the presence of blocking groups on the electrochemical properties and stability of the radical ions was demonstrated. An unusually large splitting (>1 V) was seen between the first and second oxidation and reduction waves, compared to smaller splittings (∼0.5 V) observed for most aromatic compounds. Electronic structure calculations have identified this difference as coming from the gas-phase electronic distributions in the presence of heteroatoms in BODIPY dyes. An ECL spectrum was generated for all systems, with the ECL properties directly related to the structure of the BODIPY dyes and the chemical stability of the products of electron transfer.

Acknowledgment. We thank the Center of Electrochemistry, Roche Inc., and the Robert A. Welch Foundation (F-0021) for the support of this research and Andy Tenysson for assistance with THF purification. P.J.R. is grateful for support from the National Science Foundation (CHE-0910499) and the Robert A. Welch Foundation (F-0019).

Supporting Information Available: Additional figures and experimental information. This material is available free of charge via the Internet at http://pubs.acs.org.

JA108108D

(68) Kohn, J. E.; Plaxco, K. W. *Proc. Natl. Acad. Sci. U.S.A.* **2005**, *102*, 10841–10845.
(69) Farinas, J.; Verkman, A. S. *J. Biol. Chem.* **2005**, *274*, 7603–7606.
(70) Tani, H.; Miyata, R.; Ichikawa, K.; Morishita, S.; Kurata, S.; Nakamura, K.; Tsuneda, S.; Sekiguchi, Y.; Noda, N. *Anal. Chem.* **2009**, *81*, 5678–5685.
(71) Miao, W. *Chem. Rev.* **2008**, *108*, 2506–2553.
(72) Richter, M. *Chem. Rev.* **2004**, *104*, 3003–3036.
(73) Santhanam, K. S. V.; Bard, A. J. *J. Am. Chem. Soc.* **1965**, *87*, 139–140.
(74) Faulkner, L. R.; Bard, A. J. In *Electroanalytical Chemistry*; Bard, A. J., Ed.; Marcel Dekker: New York, 1977; Vol. 10, p 1.